Received: 20 September 2022 | Revised: 12 January 2023 | Accepted: 14 January 2023

DOI: 10.1002/app.53690

RESEARCH ARTICLE

Applied Polymer SCIENCE WILEY

Polymer-based separator for all-solid-state batteries produced by additive manufacturing

Katrin Wudy[1] | **Svitlana Sapishchuk**[1] | **Joseph Hofmann**[1] | **Jochen Schmidt**[2] | **Fabian Konwitschny**[3] | **Hans-Christoph Töpper**[3] | **Ruediger Daub**[3]

[1]TUM School of Engineering and Design, Professorship of Laser-based Additive Manufacturing, Technical University of Munich, Garching, Germany

[2]Institute of Particle Technology, Friedrich-Alexander-University Erlangen-Nuernberg, Erlangen, Germany

[3]TUM School of Engineering and Design, Institute for Machine Tools and Industrial Management, Technical University of Munich, Garching, Germany

Correspondence
Katrin Wudy, TUM School of Engineering and Design, Professorship of Laser-based Additive Manufacturing, Technical University of Munich, Boltzmannstrasse 15, 85748 Garching, Germany.
Email: katrin.wudy@tum.de

Abstract

The high demand for an efficient energy supply for various applications facilitates the development of innovative storage technologies like all-solid-state batteries in addition to novel production technologies. Compared to the conventional manufacturing process, additive manufacturing (AM) is a promising technology used for the rapid and cost-effective production of battery components containing separators. However, AM technologies like laser-based powder bed fusion of polymers (PBF-LB/P) have been neglected so far. The present research aims to fill this research gap and outline a novel approach for processing polymers like polyethylene oxide (PEO) and polyvinylidene fluoride (PVDF) into separators using PBF-LB/P. Optimal process parameters for manufacturing PVDF and PEO with PBF-LB/P to generate homogeneous and dense layers represent the key findings of this paper and provide a deeper process understanding. The first proof of concept for producing separator layers by PBF-LB/P in a scalable process is demonstrated as a result.

KEYWORDS

additive manufacturing, all-solid-state battery, laser-based powder bed fusion of plastics, PVDF powder, separator

1 | INTRODUCTION

Given that conventional lithium-ion batteries (LIBs) tend to reach their physicochemical limit concerning energy storage capacity,[1] the focus is shifting increasingly toward novel energy storage technologies, such as all-solid-state batteries (SSBs). The main difference between the conventional LIB and the SSB is that of using a solid-state electrolyte (SSE) instead of a liquid electrolyte to serve as the separator and enable ionic conductivity within the electrodes.[2] The materials applied for SSE are based on polymers or inorganic materials, for example, oxides and sulphides.[3,4] The mechanical and chemical stability of the separator enables the use of a lithium metal anode consisting of a thin film of pure metallic lithium on a current collector and featuring a more compact battery design,[5] which results in a significant increase in both volumetric and gravimetric energy density. In addition, SSBs might possess further advantages regarding safety,[6,7] durability,[8,9] and enable tapping into new application fields.[10,11]

The conventional process chain (Figure 1a) adapted from the LIB production is used to produce thin-film

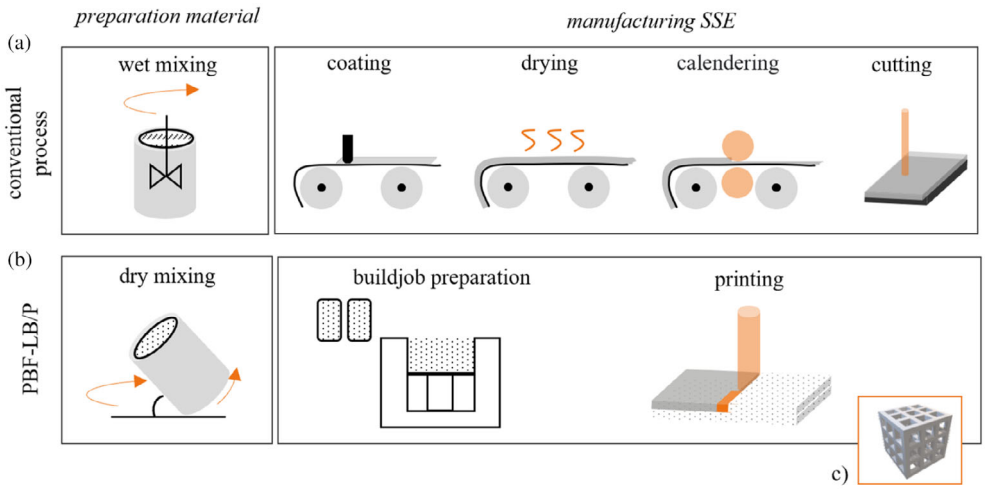

FIGURE 1 Process chain for solid-state electrolyte (SSE) manufacturing by (a) conventional route (solution casting), (b) laser-based powder bed fusion of polymers (PBF/LB-P), (c) possible SSE geometry. [Color figure can be viewed at wileyonlinelibrary.com]

polymer separators using solution casting, which consists of coating, drying, calendaring, and cutting process steps. These process steps have mainly been conducted manually, on a laboratory scale.[12–14] First, the electrolyte solution, that is, a viscous mixture of organic solvent, polymer powder, and conducting salt, is applied to the previously manufactured electrodes, and then dried. The resulting electrode separator compound is compacted and cut to the desired geometrical dimensions afterwards.[15] The dimensions thereby currently measure the range of a few millimeters.[12,16] The disadvantage of this process route is the long process chain, with sequential process steps interrelating with each other and being prone to create errors. Another disadvantage is the use of often toxic solvents which cannot be reused.

The need for novel production techniques for SSBs has drawn increasing research attention to the area of additive manufacturing (AM) because it is suitable for the solvent-free production of large-scale and dense solid layers performed in a single step.[17] Moreover, conventional fabrication by both solution casting and hot pressing as well as calendering are limited to planar geometries. In contrast, AM offers new possibilities for exploring three-dimensional SSB structures,[18] which provide new opportunities to maximize the share of the energy-storing active material, thus directly contributing to increasing the energy density of an SSB cell.[17,19] The separator was successfully produced using established AM processes, for example, material extrusion (MEX)[20,21] or vat photopolymerization (VPP).[22] Maurel et al.[20] investigated the printability of PEO/LiTFSI filaments with MEX and demonstrated varying ionic conductivity for different printing directions which was due to varying orientations of the polymer chain, which is a main drawback of MEX. Wang et al.[21] used MEX as manufacturing technology to fabricate the "textile" for a flexible all-fiber LIB. They printed an LFP (lithium iron phosphate) fiber cathode and a lithium titanium oxide (LTO) fiber anode with a gel polymer which, by twisting the created textile, becomes a quasi-solid electrolyte intended to be used for future wearable electronic applications.

In contrast, the laser-based powder bed fusion of polymers (PBF/LB-P) has not yet been researched, although it might enable simplified material preparation without the addition of the toxic solvents used in conventional manufacturing processes[23] and may offer the option of producing high-quality, post-processing-free components in a nearly one-step manufacturing process (Figure 1b).[24] PBF-LB/P is an AM technology at the highest maturity level, so it is most relevant to several industrial applications.[25] Therefore, compared to the state-of-the-art production route (solution casting), PBF-LB/P would enable solvent-free manufacturing of SSE with fewer process steps and higher geometrical freedom.

In PBF-LB/P, a polymer powder with an average particle diameter of around 60 μm[26] is selectively melted using a laser, resulting in a single dense layer of the part being produced. This step is repeated until the complete component is built, layer by layer. Intensive research has been performed regarding new materials for the PBF-LB/P process because it possesses a high potential in terms of geometrical flexibility and scalability. The polymer powder feedstock most studied is PA12.[26] However, the requirements for the feedstock material are very high in this case.[27] The material must have a defined and narrow particle size distribution and an average particle diameter of 60 μm, a smooth particle surface, a wide processing window (temperature interval between the onset of crystallization and onset of melting), and, as a result, defined thermal as well as optical behavior (since the energy input is via a laser beam source).[27]

Novel material developments have taken place in the areas of polypropylene, polyamide 6,[28] polyoxymethylene,[29] polybutylene terephthalate,[30] and poly(L-lactide).[31] Unfortunately, none of these polymers are suitable candidates for separators, as compared to those materials used in the conventional manufacturing process. The semicrystalline polymer most commonly used in SSB research is based on polyethylene oxide (PEO) by its comparatively high-

ionic conductivity, and non-existent toxicity.[32] PEO-based polymer electrolytes exhibit a high degree of crystallinity and, thus, a low-ionic conductivity at room temperature[33,34] since the so-called "hopping mechanism" of the lithium ions within the polymer is mainly driven within the amorphous phase.[35,36]

The addition of ceramic fillers and plasticizers into the polymer matrix is an effective method for increasing conductivity.[37,38] As a result, blended polymers have been investigated as SSE materials, for example, poly(ethylene oxide)/polyacrylonitrile (PEO/PAN),[39] poly(vinylidene fluoride–co–hexafluoropropylene) (PVDF-co-HFP)/poly(aniline),[40] and poly(vinyl chloride)/poly(ethyl methacrylate).[41]

Another polymer used as material for SSE is PVA, of its excellent processing behavior and chemical resistance.[42] Nevertheless, the main drawback of PVA is its low-ionic conductivity.[43] Another polymer commonly used for the fabrication of separators is polyvinylidene fluoride (PVDF).[44] In contrast to PEO and PVA, PVDF possesses high-electromechanical stability, even without fillers, and can exhibit high-ionic conductivity at room temperature.[45] Both PVDF and PEO have already been processed into separators using AM processes, for example, MEX[14,15] or material jetting (MJT).[46] However, to facilitate the PBF-LB/P process as a manufacturing technology for SSE, the polymer has to be a powder with very defined properties, and the manufacturing of dense separator layers by PBF-LB/P from PEO and PVDF with PBF-LB/P has not been possible due to the lack of powder feedstock. This article addresses groundbreaking research on the manufacturing of novel materials using PBF-LB/P technology and its application as an SSE. The present contribution seeks to outline suitable material and processing parameters used for manufacturing polymer-based separators using PBF-LB/P, and it quantifies the interdependency between product quality and processing.

2 | METHODOLOGY

2.1 | Powder mixtures as feedstock material

The feedstock material used for the PBF-LB/P process is a powder blend, with a polymer as the main component, and an active ingredient (lithium-containing conducting salt) used as an additive. The specimen prepared using the powder mixture represents a separator. However, the powder material is processed both, with and without the active ingredient.

2.1.1 | Polyvinylidene fluoride

PVDF pellets with the tradename Dyneon Fluoroplastic PVDF 6008/0001 (3 M Deutschland GmbH, Germany) were used as feedstock material for the thermally induced precipitation process using benzaldehyde as a solvent (for synthesis, Carl Roth GmbH + Co. KG, Germany).[47,48] The mechanism of the thermal precipitation process and its process parameter dependencies is not the subject of this work, and a comprehensive discussion on these aspects can be found in, for example, Refs. 29–31. Briefly, during the first step of thermally induced precipitation the thermoplastic is dissolved at elevated temperatures in a moderate solvent, which is a non-solvent at ambient temperature, but acts as a good solvent at elevated temperatures. This process is preferably performed in a stirred autoclave equipped with capabilities for cooling and heating. Starting from the state of the homogeneous solution, the stirred polymer-solvent system is then cooled down. At a characteristic temperature depending on the system's material composition, a miscibility gap is reached, and a liquid–liquid dispersed two-phase system consisting of polymer-rich droplets in a polymer-lean continuous solvent phase is formed. Upon further cooling, the polymer in the polymer-rich droplets is supersaturated, and particle nucleation and particle growth (crystallization) set in. Depending on the system composition (polymer content) and stirring conditions, particles with a narrow size distribution can be obtained in a size ranging from microns to several tens of micrometers.

Precipitation of PVDF powder was performed in a stirred autoclave having a volume of 3 liters (Büchi Labortechnik GmbH, Germany), as described in detail in Ref. 30. The autoclave enables process temperatures of up to 300°C and pressures of up to 200 bar. The jacket of the autoclave is equipped with an electrical heating and a cooling coil feed with water of about 14°C. PVDF and benzaldehyde were introduced into the reactor system. The autoclave was flushed with nitrogen (N_2), closed, and pressurized to 2 bars. The polymer concentration measured 10 wt.-% (total mass of the PVDF/benzaldehyde system is 2.3 kg). The mixture was heated while being stirred at 500 min^{-1} to 200°C, kept at this temperature for 15 min, and cooled down at 3 K/min to 60°C. The precipitation product was separated from the solvent via filtration and washed using denatured ethanol and deionized water to remove the solvent. The product was dried in an oven at 130°C for at least 24 h. To obtain particles having beneficial flowability, the dried product was deagglomerated in a Pulverisette-14 rotor mill (Fritsch GmbH, Germany), which was operated at idle speed and equipped with a 0.5 mm sieve ring. The obtained powder was dry coated with 0.1 wt.-% fumed silica, similar to a tubular mixture in the procedure described in Ref. 30. The dry-coated PVDF powder was analyzed regarding its particle size distribution and thermal behavior to investigate the potential PBF-LB/P processing behavior.

2.1.2 | Polyethylene oxide

PEO with a molecular weight of 100.000 g/mol from Sigma Aldrich (Sigma Aldrich Corp., Germany) was used as the second polymer for the PBF-LB/P experiments. To improve the ionic conductivity and increase the mechanical stability of the manufactured separator,[4] 5 wt.-% of aluminum oxide (Al_2O_3) nanoparticles from Sigma Aldrich (Sigma Aldrich Corp., Germany) are added to the PEO powder using a dual asymmetric centrifuge rotary mixer (type: Speedmixer DAC 1100.2 VAC-P, Hauschild GmbH & Co. KG, Germany). The homogeneous distribution of Al_2O_3 nanoparticles on the surface of the PEO particles is ensured by scanning electron microscopy (SEM) and energy dispersive X-ray analysis (EDX), although scattered insignificant Al_2O_3 agglomerates can be detected.

2.1.3 | Lithium perchlorate

The choice of a conducting salt comes down to lithium perchlorate ($LiClO_4$). Compared to fluorine-containing conducting salts such as LiTFSI (lithium bis(trifluoromethanesulfonyl)imide), $LiClO_4$ is less sensitive to atmospheric moisture,[32] which facilitates the processing in a PBF-LB/P system under ambient conditions. Since $LiClO_4$ is physically in the form of coarse granules, it is comminuted into smaller particles using a planetary micro mill (Pulverisette premium line, Fritsch GmbH, Germany).

To produce a separator providing sufficient ion conductivity, the conducting salt $LiClO_4$ must be homogeneously incorporated into the polymer matrix, which consists of either PVDF or PEO. The addition of 1.97 wt.-% (or a ratio of 8:1) of $LiClO_4$ into either a PVDF or PEO polymer matrix and 5 wt.-% of Al_2O_3 is performed using a planetary micro mill (Pulverisette 7 premium line, FRITSCH GmbH, Germany). The explosiveness of $LiClO_4$ must be considered when mixing, as perchlorate is a strong oxidizing agent, which is why $LiClO_4$ is considered to be explosive at elevated temperatures and in combination with organic materials.[32] 9 g of the mixture is gently blended with an effective mixing time of 60 min and at a mixing speed of 100 min^{-1}.

2.2 | Material and specimen characterization

Chatham et al. listed the following as crucial parameters for a successful PBF-LB/P process in ref. 27: the particle size distribution, the Hausner ratio (value for powder flowability), the sphericity, the thermal properties (crystallization and melting temperature, melting enthalpy), the optical absorption behavior, the viscosity, and the surface tension. The Hausner ratio (an indicator of powder flowability), the particle size distribution, and the thermal properties of the feedstock material are determined before manufacturing to estimate the process behavior. The surface morphology and the distribution of the active material are investigated on the single-layer specimen.

2.2.1 | Powder flowability

The bulk density ρ_{bulk} and the Hausner ratio (H_R) represent powder characteristics relevant to PBF-LB/P and are correlated with the final specimen density.[44] The bulk density ρ_{bulk} is determined as per DIN EN ISO 60 using a bulk density tester (Emmeram Karg Industrietechnik, GmbH), and the tapped density ρ_{tap} is determined following DIN EN ISO 787-11 using a graduated cylinder. H_R is calculated according to the following equation:

$$H_R = \frac{\rho_{tap}}{\rho_{bulk}}. \quad (1)$$

2.2.2 | Particle size distribution

The particle size distribution of PEO is measured via laser diffraction (Mastersizer 3000, Malvern Panalytical Ltd., United Kingdom). The PVDF particles were also measured via laser diffraction, but in aqueous dispersion (Mastersizer 2000, Malvern Panalytical Ltd., United Kingdom). The results of the particle size distribution are presented as per DIN ISO 9276-1. The values $d_{10,3}$; $d_{50,3}$; and $d_{90,3}$ are percentile values indicating the particle sizes below 10%, 50%, and 90% of all particles analyzed.

2.2.3 | Differential scanning calorimetry

Differential scanning calorimetry (DSC) is a measuring method used for determining the thermal properties of polymers as per DIN EN ISO 11357-2. For the thermal characterization of the PVDF and PEO powders, a sample with a mass of 10 mg was heated from 20 to 210°C (PVDF) and 90°C (PEO) at a heating rate of 10 K/min and then cooled to 20°C at a cooling rate of 10 K/min.

TABLE 1 Processing parameters on Formiga P100

PEO + 5 wt.-% Al_2O_3					
Process parameter	**T_B (°C)**	**P_L (W)**	**v_s (mm/s)**	**h_s (mm)**	**E_D (J/mm²)**
$P_L3\_v_s1000\_h_s0.1\_E_D0.03$	70	3	1000	0.1	0.03
$P_L3\_v_s900\_h_s0.1\_E_D0.033$	70	3	900	0.1	0.033
$P_L3\_v_s800\_h_s0.1\_E_D0.038$	70	3	800	0.1	0.038
$P_L3\_v_s700\_h_s0.1\_E_D0.043$	70		700	0.1	0.043
PVDF					
$P_L6\_v_s1050\_h_s0.2\_E_D0.029$	167	6	1050	0.2	0.029
$P_L6\_v_s900\_h_s0.2\_E_D0.033$	167	6	900	0.2	0.033
$P_L4\_v_s700\_h_s0.2\_E_D0.029$	167	4	700	0.2	0.029
$P_L64\_v_s600\_h_s0.2\_E_D0.033$	167	4	600	0.2	0.033

Abbreviations: E_D, energy density; h_s, hatch distance; PEO, polyethylene oxide; P_L, laser power; PVDF, polyvinylidene fluoride; T_B, building chamber temperature; v_s, scan velocity.

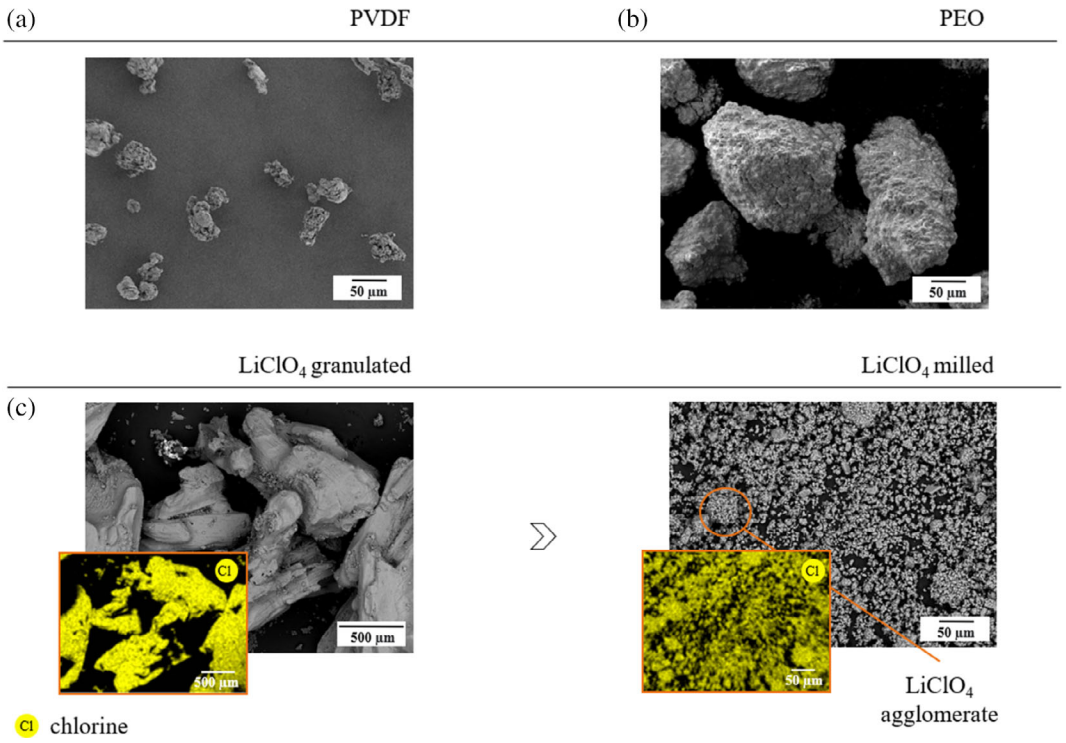

FIGURE 2 Scanning electron microscopy (SEM) images of (a) polyvinylidene fluoride (PVDF) and (b) polyethylene oxide (PEO) particles, as well as SEM images and energy dispersive X-ray (EDX) analysis of (c) $LiClO_4$ distribution before and after the milling process. [Color figure can be viewed at wileyonlinelibrary.com]

2.2.4 | Scanning electron microscopy

The SEM images and EDX analyses are prepared by using a microscope with tungsten cathode (type: JSM-IT200, JEOL GmbH, Germany). EDX analysis is used to determine the elemental composition of the powder and the manufactured sample. All measurements are performed using a secondary electron detector (SED) as the source of information at acceleration voltages between 5 and 15 kV.

2.2.5 | Confocal laser scanning microscope

Laser scanning microscope (LSM) is used for contact-free measurement of the surface morphology and the

TABLE 2 Main material characteristics, including (a) characteristic particle sizes and (b) powder flowability

(a) Particle sizes	PVDF	PEO	
$d_{10,3}$ (µm)	43	10	
$d_{50,3}$ (µm)	50	158	
$d_{90,3}$ (µm)	150	1950	
(b) Powder flowability	**PVDF**	**PEO**	**PEO + 5 wt.-% Al_2O_3**
ρ_{bulk} (g/cm^3)	0.51 ± 0.006	0.45 ± 0.002	0.57 ± 0.002
H_R (−)	1.11 ± 0.005	1.15 ± 0.008	1.13 ± 0.003

Abbreviations: PEO, polyethylene oxide; PVDF, polyvinylidene fluoride.

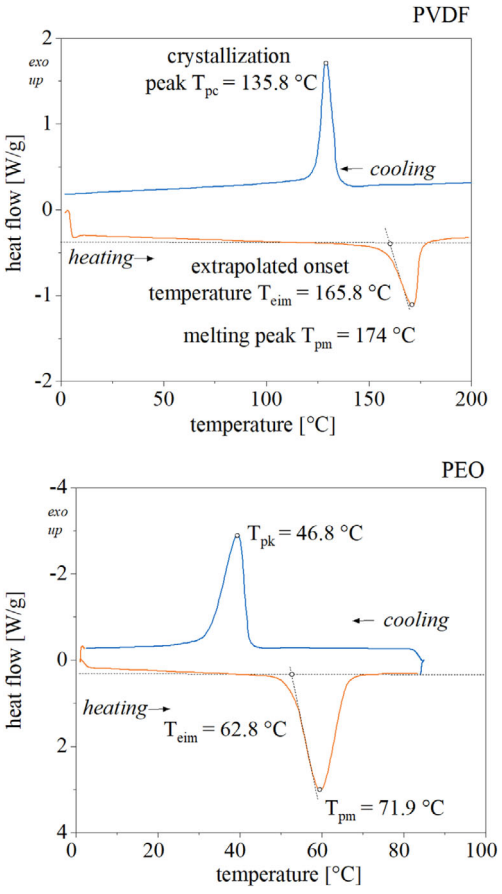

FIGURE 3 Differential scanning calorimetry (DSC) measurements of polyvinylidene fluoride (PVDF) and polyethylene oxide (PEO). [Color figure can be viewed at wileyonlinelibrary.com]

roughness of the PBF-LB/P specimens. The surface quality of the manufactured specimens is measured using a laser scanning microscope (type: VK-X1000, Keyence Deutschland GmbH, Germany). The arithmetic average line roughness R_a and mean line roughness depth R_z are calculated as per DIN EN ISO 4288 at a measuring length l_n of 4 mm and a cut-off length λ_c of 0.8 mm, by spacing 30 lines 15 pixels apart. The waviness of the specimens caused by temperature-induced curling is eliminated for visualization. The resulting single-layer specimen thickness d is measured using a screw gauge.

2.3 | Powder bed fusion of plastics as the manufacturing process

Melt pool formation is a consequence of the interaction between laser radiation and the powder bed and is thus determined by process settings. The most relevant process settings in PBF-LB/P are the hatch distance (the distance between two laser lines), the laser power, and the scan speed.[45] One common procedure used for developing novel powders and evaluating optimal process parameters is that of manufacturing single layers to fundamentally understand the interaction between laser and material before fine-tuning the process settings.[46]

The experiments are performed on a PBF-LB/P setup (Formiga P100, EOS GmbH, Germany). The machine is equipped with a 30 W CO_2 laser (wavelength: 10.6 µm). A single-layer specimen with dimensions of 12 × 12 mm^2 and a layer thickness of 0.1 mm is used for the experiments.

The process parameters are determined according to a previously performed process parameter screening and listed in Table 1. For PEO + 5 wt.-% Al_2O_3, the processing parameters of laser power P_L, hatch distance h_S, and layer thickness d are held constant, while the scan speed v_S is ranging between 700 and 1000 mm/s. For PVDF, the parameters hatch distance h_s and layer thickness d are held constant while the scan speed v_S is ranging between 600 and 1050 mm/s, and the laser power P_L varied from 6 to 4 W.

For each process parameter set, the energy density E_D is determined by the following equation:

$$E_D = \frac{P_L}{v_s \cdot h_s}. \quad (2)$$

The building chamber temperatures are determined according to the model of quasi-isothermal laser sintering[49] based on DSC measurements.

3 | RESULTS AND DISCUSSION

3.1 | Suitability of feedstock material for the PBF-LB/P process

Before processing with PBF-LB/P, the feedstock material is evaluated regarding its processability. Figure 2c shows

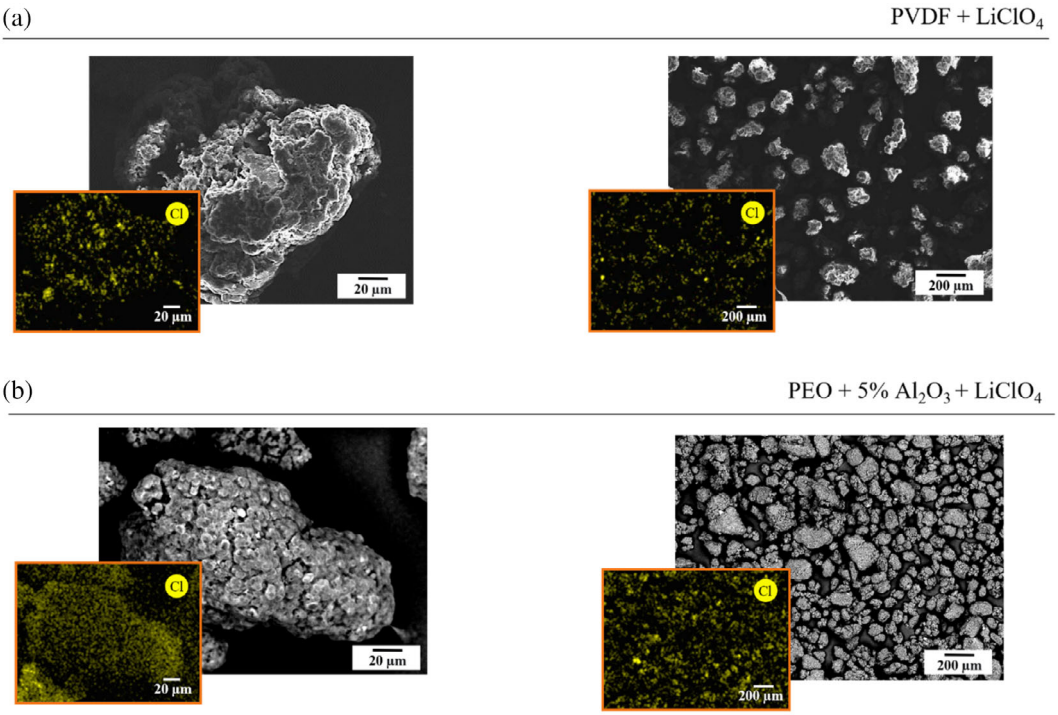

FIGURE 4 Scanning electron microscopy (SEM) images and energy dispersive X-ray (EDX) analyses after milling of (a) polyvinylidene fluoride (PVDF) + $LiClO_4$ powder mixture and (b) polyethylene oxide (PEO) + 5 wt.-% Al_2O_3 + $LiClO_4$ powder mixture. [Color figure can be viewed at wileyonlinelibrary.com]

$LiClO_4$ before and after the milling process. The addition of $LiClO_4$ is essential as it is advantageous to increase the ionic conductivity of the SSE and the produced separator.[50] Thus, a homogenous distribution of $LiClO_4$ is required. Figure 2 shows the precipitated PVDF powder particles, which have an irregular shape and an average particle size $d_{50,3}$ of around 50 µm. Compared to PVDF, the PEO particles exhibit a "potato-like shape" with a rough surface morphology and an average particle size of around 150 µm (Figure 2b). Considering a typical layer thickness in PBF-LB/P of 100 µm, the PEO particle size may lead to challenges during processing since the particle size would be higher than the layer height. The broad particle size distribution of PEO is illustrated in Table 2 (a), where characteristic particle size values are plotted. In comparison, conventionally applied powders possess a particle size distribution with a $d_{10,3}$ of 20 µm and a $d_{90,3}$ of 80 µm.[44] This powder characteristic can strongly influence both the density of the manufactured specimen[51] and its layer thickness.[52] A comparison of the two materials reveals a more suitable particle size distribution of the PVDF powder for the PBF-LB/P process. The $d_{50,3}$ in particular is in the range of commercial PBF-LB/P powders like PA12.[53]

In addition, Table 2 (b) contains the powder flowability of the feedstock material. H_R values below 1.15 are considered optimal and indicate an easily flowing bulk material.[53] Greater flowability is directly related to the quality of the powder bed after the coating process, and thus the density of the specimen.[27] The Hausner ratio of both powders is below 1.15, thus indicating a sufficient flow behavior and advantageous coating behavior during processing.

Figure 3 shows the results of DSC measurements and provides information about the thermal properties of the polymers. The latter are of main interest regarding the process, or rather the building chamber temperature. The temperature difference between the onset of melting and the onset of crystallization determines the thermal processing window and the adjustment of the building chamber temperature. Since there is a temperature distribution on the build surface, it is a common procedure to set the preheating temperature to be near the onset of the melting temperature.

The processing temperature range for PVDF is between 145 and 166°C, and for PEO between 51 and 63°C. The set temperature in the PBF-LB/P system during the manufacturing process is 167°C for PVDF and 70°C for PEO. However, the actual surface temperatures measured using the thermocouple are 165 and 55°C, respectively. The main reason for the difference between contact and contact-free temperature measurements is

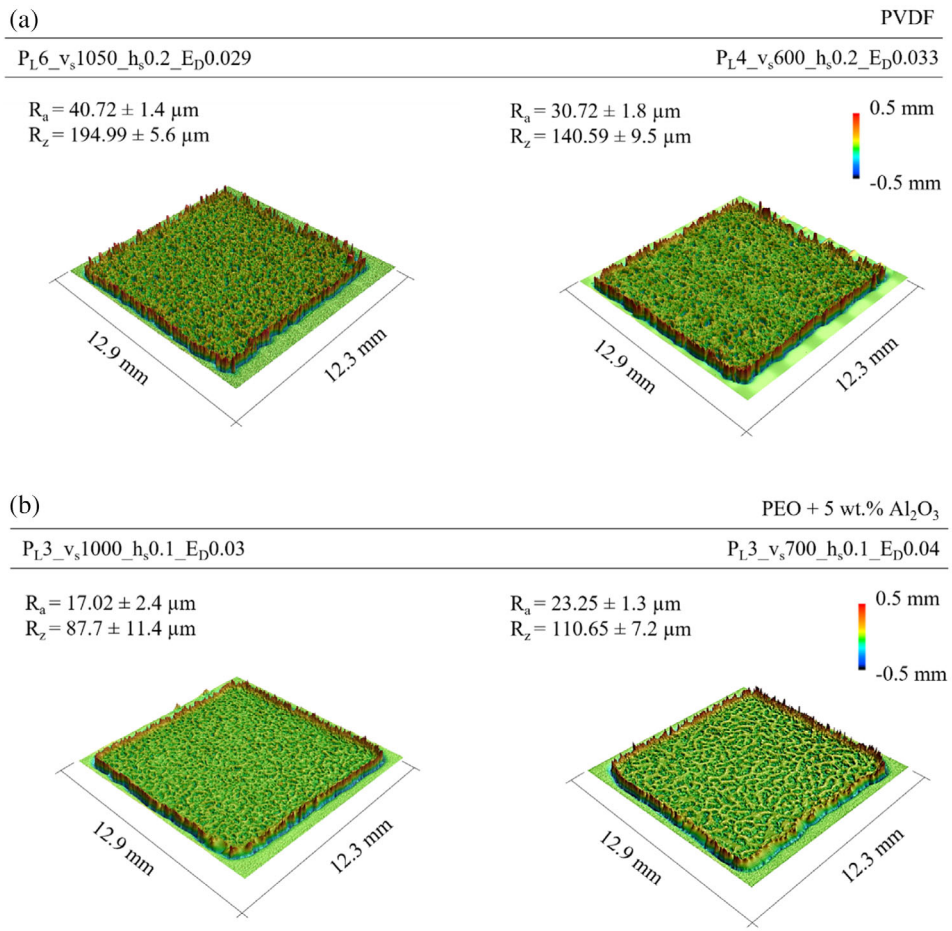

FIGURE 5 Laser scanning microscope (LSM) visualization of the surface morphology; R_a, R_z, and d of specimens manufactured from (a) pure polyvinylidene fluoride (PVDF) and (b) polyethylene oxide (PEO) + 5 wt.-% Al_2O_3. [Color figure can be viewed at wileyonlinelibrary.com]

mainly attributed to several heat fluxes and measurement errors (unknown emissivity), which are not considered to be relevant in this case.

The distribution of the conductive lithium salt is evaluated using EDX analyses. The color-coded elemental distribution resulting from the EDX (Figure 4) shows that the chlorine, as part of $LiClO_4$, is uniformly distributed over the surface of the PEO and PVDF particles. The milled $LiClO_4$ coating of the feedstock particles was able to be explained by adhesion forces.[27] Nevertheless, it appears that the presence of localized agglomerations cannot be excluded entirely. The addition of $LiClO_4$, however, seems to have changed the morphology of the PEO + 5 wt.-% Al_2O_3 powder mixture. This outcome is especially reflected in the flow properties of the powder (Table 2, b) and it is also evident in the lower surface quality of the powder bed after the coating process, as characterized by the homogeneity of the thickness and presence of defects. This is not necessarily attributable to the addition of $LiClO_4$, but may rather have been caused by the change in the shape and arrangement of the PEO particles during the milling process.[27] Since such incorporation of $LiClO_4$ into the polymer matrix is being practiced,[54] and agglomeration of the active ingredients cannot be excluded even in conventional SSE separator production, the addition of $LiClO_4$ is considered satisfactory.

3.2 | PBF-LB/P of the PVDF and PEO powders

Before processing the powder mixture containing the conducting salt, the most suitable process parameters are selected from the process parameter screening of the feedstock material. The energy density spectrum of the selected parameters falls in the range between 0.025 and 0.045 J/mm^2. According to several studies on various materials, this range is considered optimal for processing polymers with PBF-LB/P.[55]

After the manufacturing of the single layers, their surface roughness is analyzed to ensure that a homogeneous melt pool has been formed, which is a basic requirement for the subsequent multi-layer process. The surface roughness of single layers after exposure depends on numerous factors, for example, powder quality,[56,57] component orientation,[58] and process parameters.[59,60] Regarding the development of novel powders and their initial processing, it is common practice to manufacture single layers and

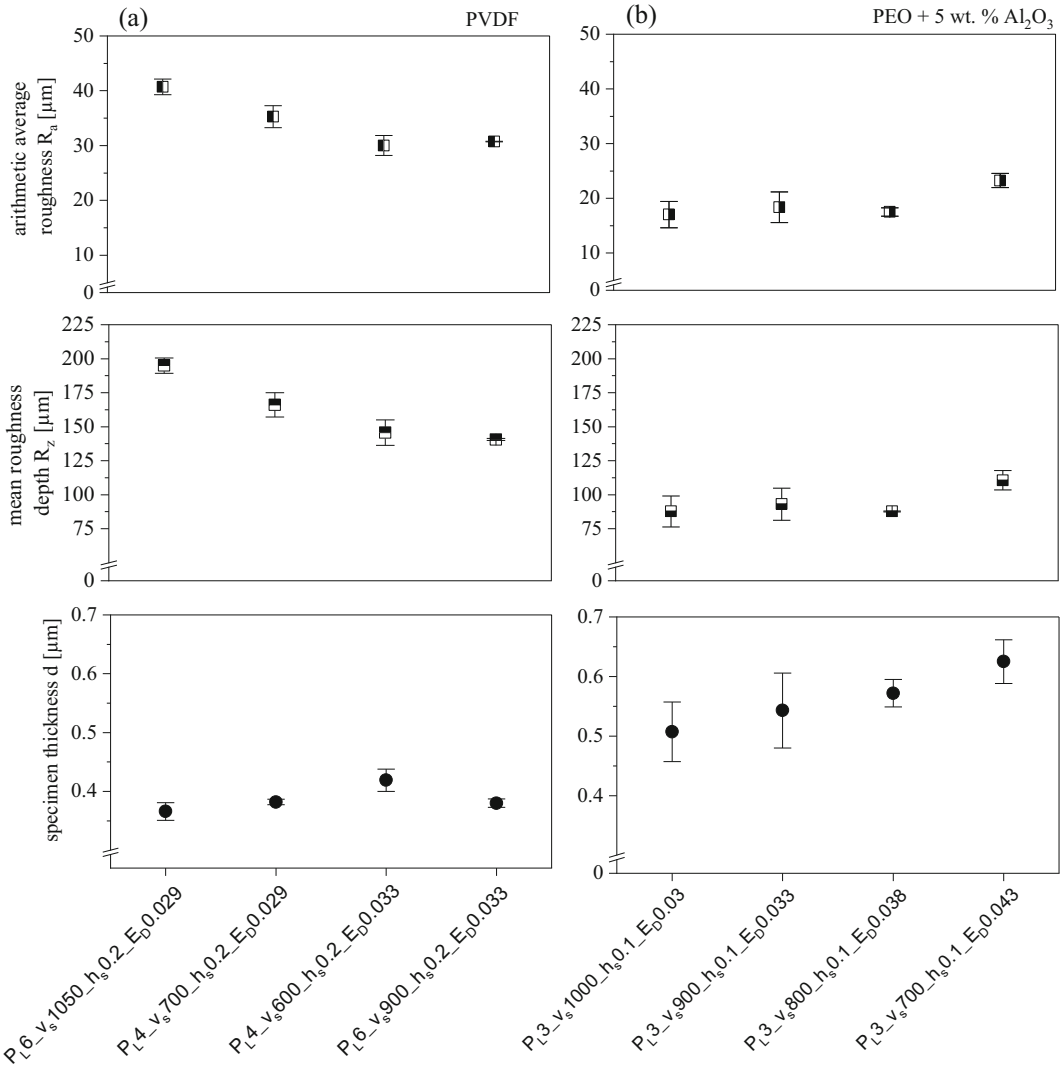

FIGURE 6 R_a, R_z, and d of the specimens manufactured from (a) polyvinylidene fluoride (PVDF) and (b) polyethylene oxide (PEO) + 5 wt.-% Al_2O_3 for different process parameters.

analyze the specific properties of these layers. Doing so can provide insights into the fundamental laser-material interaction and melting behavior. Since all the other factors influencing the single-layer roughness remained constant in the present study, the differences in surface roughness can be attributed to the influence of the process parameters. Figure 5 shows the morphology of the specimen manufactured from PVDF. Specimens manufactured at the lowest energy density E_D of 0.029 J/mm^2 exhibit a rougher surface compared to such manufactured with a higher energy density E_D of 0.033 J/mm^2. These visual observations are also reflected in the surface roughness values. A higher energy density typically leads to a higher temperature during laser exposure, which goes along with a decreased viscosity of the polymer and a faster coalescence. Nevertheless, too high-energy densities may initiate degradation effects or overheating, which may have negative effects on the single-layer surface quality and component properties. This is observed for PEO. Figure 5b shows the morphology of the specimen manufactured from PEO + 5 wt.% Al_2O_3 and presents the opposite situation.

Specimens manufactured at a higher energy density E_D of 0.038 J/mm^2 exhibit a rougher surface than those manufactured at a lower energy density E_D of 0.030 J/mm^2. At an increasing laser power P_L, and consequently rising energy density, the line roughness R_a and R_z tend to increase (see Figure 6). Maintaining a uniform morphology and minimal roughness is essential, as insufficient interfacial contacts between the electrodes and the SSE separator is a major factor able to negatively affect the overall performance of the SSB.[36] The lack of contacts leads to a high-interfacial resistance, which impairs ion transport, limits charging and discharging

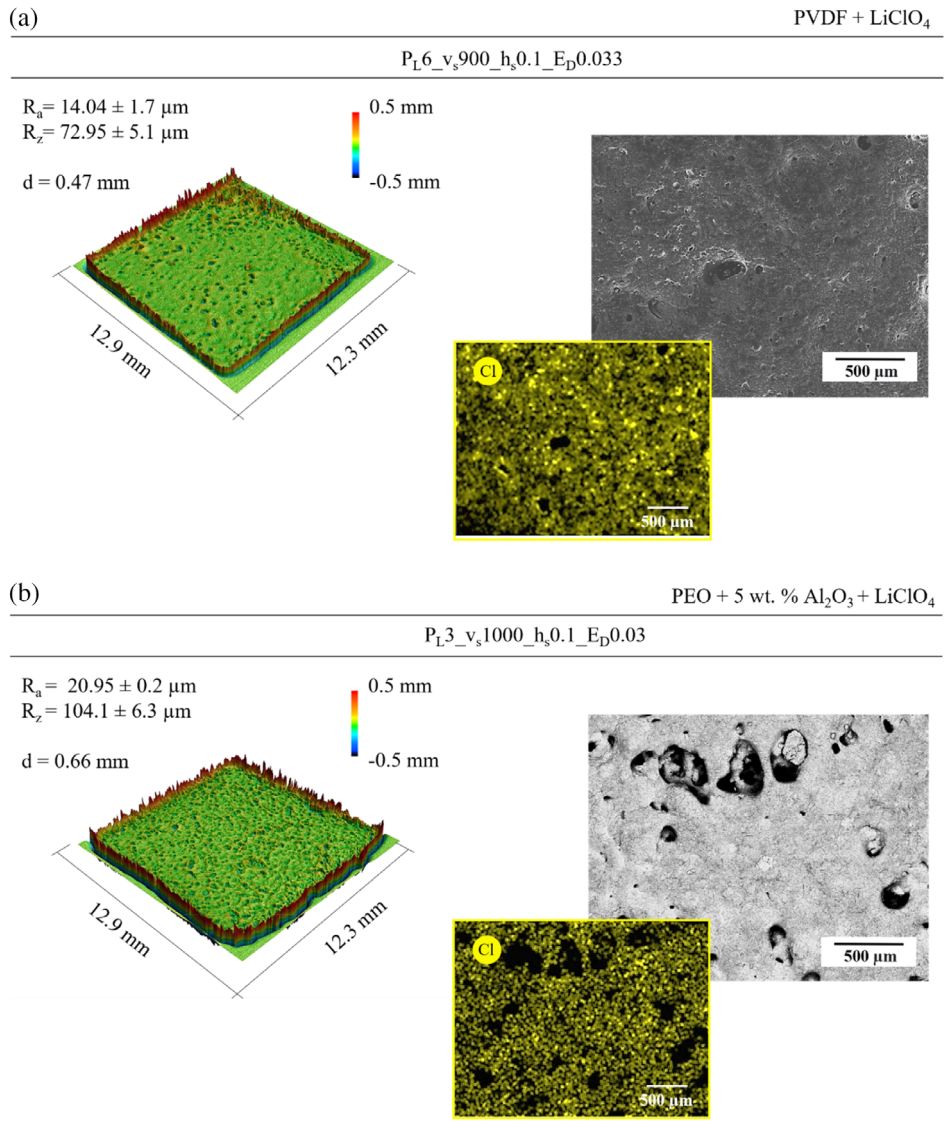

FIGURE 7 (a) Laser scanning microscope (LSM) visualization of specimen surface roughness, scanning electron microscopy (SEM), and energy dispersive X-ray analysis (EDX) of manufactured separators based on (a) polyvinylidene fluoride (PVDF) + $LiClO_4$ and (b) polyethylene oxide (PEO) + 5 wt.-% Al_2O_3 + $LiClO_4$. [Color figure can be viewed at wileyonlinelibrary.com]

speed, and increases the risk of lithium dendrite growth.[4,12]

The thickness *d* of a single layer specimen can range from 150% to 180% of the layer height value (100 µm) specified in the system.[44] The resulting thickness of specimens manufactured from PEO + 5 wt.-% Al_2O_3 and PVDF significantly exceeded this specification (see Figure 6). This outcome may have been related to the particle size distribution (Table 2, a), as a larger particle size leads to larger void volume in the powder bed, thus causing the beam to be absorbed by deeper-lying particles, which increases the penetration depth.[55]

As researchers have already observed, the thickness of a single layer also increases with rising energy density E_D.[56–58] This correlation is also observed for PEO + 5 wt.-% Al_2O_3 (Figure 4b). However, this assumption cannot be confirmed for PVDF, so it is necessary to consider certain process parameter sets to achieve the desired separator thickness. In a conventional solid-state separator manufactured under laboratory conditions, the average thickness is reported to be about 100 µm.[57] However, the target thickness needed in an SSB application to compete in terms of energy density is less than 30 µm.[15]

3.3 | Separator manufacturing

The processability of PEO and PVDF, as relevant materials for the separator and catholyte of SSBs, using PBF-LB/P was demonstrated in the previous section. To the best of the authors' knowledge both feedstock materials have never been processed by PBF-LB/P manufacturing technology. Following to the successful proof of concept a conducting lithium salt must be added to the feedstock material to produce a separator that is usable for SSBs.

The stated goal for the final specimens manufactured using PBF-LB/P is to achieve a smooth surface so that the interfacial contacts, and, thus, exchange current density between the separator and the electrodes of the battery cell, can be maximized. Given that the process parameter sets "$P_L4\_v_s600\_h_s0.2\_E_D0.033$" for PVDF and "$P_L3\_v_s1000\_h_s0.1\_E_D0.03$" for PEO + 5 wt.-% Al_2O_3 show the best results in terms of surface morphology and the resulting specimen thickness, these sets are used for separator manufacturing. Figure 7 illustrates separators specimen fabricated using PBF-LB/P from PVDF + $LiClO_4$ and PEO + 5 wt.-% Al_2O_3 + $LiClO_4$. The SEM and LSM visualizations show that the morphology of the samples exhibits complete particle coalescence. The surface roughness, especially that of the PVDF + $LiClO_4$, was even smoother than for the specimen produced with PVDF. Furthermore, the color-coded EDX analysis confirms the homogeneous distribution of chlorine as a unique indicator for the conducting salt, even after the PBF-LB/P process. The present experiments demonstrate impressively that PVDF filled with conductive lithium salt is particularly suitable for processing by PBF-LB/P and, therefore, for the AM of SSB separators. Given that this study is oriented toward establishing process understanding and the identification of a suitable manufacturing strategy, only the functionality was demonstrated, and a more detailed electrochemical analysis was not conducted, but one will be conducted in the future. (Figure 7)

4 | CONCLUSION AND OUTLOOK

The present work provides insights into the PBF-LB/P processability of materials commonly used in all-SSB separator production. The main components providing mechanical integrity and acting as a matrix are PEO and PVDF, whereby $LiClO_4$ serves as a conductive additive used to enhance ionic conductivity. The incorporation of $LiClO_4$ into the polymer matrix is performed using a ball mill. An EDX analysis shows the homogeneous distribution of the active ingredient on the polymer particle surface, but sporadic agglomerates are detected. Before separator manufacturing, the final process parameters for the feedstock materials are identified by way of a PBF-LB/P parameter study. The suitability of the feedstock material for PBF-LB/P processing is ensured by analyzing key characteristics, e.g., the flowability, particle size distribution, and thermal properties of the powder. As a result, the final PVDF separators exhibit lower surface roughness and a film thickness similar to that of the PEO-based separators.

This first proof of concept on the processing of polymer materials for separators suitable for the manufacturing of SSB with PBF-LB/P has shown very successful results and will be substantiated in the future by research into both multilayer components, and composite cathodes composed of the solid electrolyte and cathode material. Since the manufacturing of components possesses geometrical dimensions beyond the laboratory scale, the procedure is highly relevant to industrial manufacturing and mass-market applications. A holistic electrochemical analysis of the components produced should follow as soon as a process understanding has been established and will provide further insights into the performance of the separators in an SSB.

In the future large format ($90 \times 115 \times 0.1\ mm^3$), polymer-based separators for SSB should be produced using PBF-LB/P. Assuming a building space of a common PBF-LB/P system (EOS P100), 1000 samples (format $90 \times 115 \times 0.1\ mm^3$) can be manufactured in a single building process, which would take 27 h. Thus, the novel PBF-LB/P process route would be highly efficient.

AUTHOR CONTRIBUTIONS

Katrin Wudy: Conceptualization (lead); methodology (lead); project administration (lead); resources (lead); supervision (equal); writing – original draft (equal); writing – review and editing (lead). **Svitlana Sapishchuk:** Data curation (lead); formal analysis (lead); investigation (lead); writing – original draft (equal). **Joseph Hofmann:** Supervision (equal); writing – review and editing (supporting). **Jochen Schmidt:** Formal analysis (supporting); investigation (supporting); writing – original draft (supporting); writing – review and editing (supporting). **Fabian Konwitschny:** Supervision (equal); writing – review and editing (supporting). **Hans-Christoph Töpper:** Formal analysis (supporting); investigation (supporting); supervision (equal); writing – original draft (supporting); writing – review and editing (supporting). **Ruediger Daub:** Resources (supporting); writing – review and editing (supporting).

ACKNOWLEDGMENT

Open Access funding enabled and organized by Projekt DEAL.

FUNDING INFORMATION

This research received no specific grant from any funding agency in the public, commercial, or not-for-profit sectors.

DATA AVAILABILITY STATEMENT

The datasets generated during and/or analysed during the current study are not publicly available but are

available from the corresponding author on reasonable request.

ORCID

Katrin Wudy https://orcid.org/0000-0002-3384-4651
Svitlana Sapishchuk https://orcid.org/0000-0003-3833-4404
Joseph Hofmann https://orcid.org/0000-0003-1122-1127
Jochen Schmidt https://orcid.org/0000-0002-9056-2749
Fabian Konwitschny https://orcid.org/0000-0002-6477-4836

REFERENCES

[1] J. Janek, W. G. Zeier, *Nat. Energy* **2016**, *1*, 1.
[2] M. Doppelbauer, *Grundlagen der Elektromobilität: Technik, Praxis, Energie und Umwelt*, 1st ed., Springer Fachmedien Wiesbaden, Wiesbaden **2020**, p. 434.
[3] F. Han, J. Yue, X. Zhu, C. Wang, *Adv. Energy Mater.* **2018**, *8*, 1703644.
[4] H. Liu, T. J. Webster, *Int. J. Nanomed.* **2010**, *5*, 299.
[5] J. R. Nair, L. Imholt, G. Brunklaus, M. Winter, *Electrochem. Soc. Interface* **2019**, *28*, 55.
[6] A. C. Luntz, J. Voss, K. Reuter, *J. Phys. Chem. Lett.* **2015**, *6*, 4599.
[7] F. Wu, W. Fitzhugh, L. Ye, J Ning, and X. Li. *Nat. Commun.* **2018**, *9*, 4037.
[8] A. Hayashi, N. Masuzawa, S. Yubuchi, F. Tsuji, C. Hotehama, A. Sakuda, M. Tatsumisago, *Nat. Commun.* **2019**, *10*, 5266.
[9] L. Froboese, L. Groffmann, F. Monsees, L. Helmers, T. Loellhoeffel, A. Kwade, *J. Electrochem. Soc.* **2020**, *167*, 20558.
[10] T. Krauskopf, H. Hartmann, W. G. Zeier, J. Janek, *ACS Appl. Mater. Interfaces* **2019**, *11*, 14463.
[11] Y. Jiang, X. Yan, Z. Ma, P. Mei, W. Xiao, Q. You, Y. Zhang, *Polymer* **2018**, *10*, 1237.
[12] R. C. Agrawal, S. A. Hashmi, G. P. Pandey, *Ionics* **2007**, *13*, 295.
[13] P. Hovington, M. Lagacé, A. Guerfi, P. Bouchard, A. Mauger, C. M. Julien, M. Armand, K. Zaghib, *Nano Lett.* **2015**, *15*, 2671.
[14] P. Han, Y. Zhu, J. Liu, *J. Power Sources* **2015**, *284*, 459.
[15] J. Schnell, T. Günther, T. Knoche, C. Vieider, L. Köhler, A. Just, M. Keller, S. Passerini, G. Reinhart, *J. Power Sources* **2018**, *382*, 160.
[16] K. Kimura, M. Yajima, Y. Tominaga, *Electrochem. Commun.* **2016**, *66*, 46.
[17] Y. Pang, Y. Cao, Y. Chu, M. Liu, K. Snyder, D. MacKenzie, C. Cao, *Adv. Funct. Mater.* **2020**, *30*, 1906244.
[18] D. W. McOwen, S. Xu, Y. Gong, Y. Wen, G. L. Godbey, J. E. Gritton, T. R. Hamann, J. Dai, G. T. Hitz, L. Hu, E. D. Wachsman, *Adv. Mater.* **2018**, *30*, e1707132.
[19] X. Wang, X. Lu, B. Liu, D. Chen, Y. Tong, G. Shen, *Adv. Mater.* **2014**, *26*, 4763.
[20] A. Maurel, M. Armand, S. Grugeon, B. Fleutot, C. Davoisne, H. Tortajada, M. Courty, S. Panier, L. Dupont, *J. Electrochem. Soc.* **2020**, *167*, 70536.
[21] Y. Wang, C. Chen, H. Xie, T. Gao, Y. Yao, G. Pastel, X. Han, Y. Li, J. Zhao, K. K. Fu, L. Hu, *Adv. Funct. Mater.* **2017**, *27*, 1703140.
[22] S.-H. Kim, J.-H. Kim, S.-J. Cho, S.-Y. Lee, *Adv. Energy Mater.* **2019**, *9*, 1901841.
[23] A. Zhakeyev, P. Wang, L. Zhang, W. Shu, H. Wang, J. Xuan, *Adv. Sci.* **2017**, *4*, 1700187.
[24] K. A. Acord, A. D. Dupuy, X. Wang, A. L. Vyatskikh, O. K. Donaldson, T. J. Rupert, J. J. Wu, Q. N. Chen, J. M. Schoenung, *J. Mater. Res.* **2021**, *36*, 4565.
[25] R. Lezama-Nicolás, M. Rodríguez-Salvador, R. Río-Belver, I. Bildosola, *Scientometrics* **2018**, *117*, 1425.
[26] I. M. Kusoglu, C. Doñate-Buendía, S. Barcikowski, B. Gökce, *Materials* **2021**, *14*, 1169.
[27] C. A. Chatham, T. E. Long, C. B. Williams, *Prog. Polym. Sci.* **2019**, *93*, 68.
[28] A. Wegner, *Phys. Proc.* **2016**, *83*, 1003.
[29] M. A. Dechet, I. Baumeister, J. Schmidt, *Materials* **2020**, *13*, 1535.
[30] M. A. Dechet, J. S. Gómez Bonilla, M. Grünewald, K. Popp, J. Rudloff, M. Lang, J. Schmidt, *Mater. Des.* **2021**, *197*, 109265.
[31] M. A. Dechet, A. Demina, L. Römling, J. S. Gómez Bonilla, F. J. Lanyi, D. W. Schubert, A. Bück, W. Peukert, J. Schmidt, *Additive Manuf.* **2020**, *32*, 100966.
[32] G. H. Newman, R. W. Francis, L. H. Gaines, B. M. L. Rao, *J. Electrochem. Soc.* **1980**, *127*, 2025.
[33] Z. Stoeva, I. Martin-Litas, E. Staunton, Y. G. Andreev, P. G. Bruce, *J. Am. Chem. Soc.* **2003**, *125*, 4619.
[34] O. Sheng, C. Jin, J. Luo, H. Yuan, C. Fang, H. Huang, Y. Gan, J. Zhang, Y. Xia, C. Liang, W. Zhang, X. Tao, *J. Mater. Chem. A* **2017**, *5*, 12934.
[35] J. Zheng, M. Gu, J. Xiao, P. Zuo, C. Wang, J.-G. Zhang, *Nano Lett.* **2013**, *13*, 3824.
[36] A. Manthiram, X. Yu, S. Wang, *Nat. Rev. Mater.* **2017**, *2*, 1.
[37] H. Wang, C. Lin, X. Yan, A. Wu, S. Shen, G. Wei, J. Zhang, *J. Electroanal. Chem.* **2020**, *869*, 114156.
[38] J.-Y. Wang, M.-C. Wang, D.-J. Jan, *Sol. Energy Mater. Sol. Cells* **2017**, *160*, 476.
[39] F. Yuan, H.-Z. Chen, H.-Y. Yang, H.-Y. Li, M. Wang, *Mater. Chem. Phys.* **2005**, *89*, 390.
[40] A. L. Ahmad, U. R. Farooqui, N. A. Hamid, *Electrochim. Acta* **2018**, *283*, 842.
[41] S. Rajendran, M. R. Prabhu, M. U. Rani, *J. Power Sources* **2008**, *180*, 880.
[42] H. A. Every, F. Zhou, M. Forsyth, D. R. MacFarlane, *Electrochim. Acta* **1998**, *43*, 1465.
[43] A. A. Mohamad, N. S. Mohamed, M. Z. A. Yahya, R. Othman, S. Ramesh, Y. Alias, A. K. Arof, *Solid State Ionics* **2003**, *156*, 171.
[44] M. Schmid, *Selektives Lasersintern (SLS) mit Kunststoffen: Technologie, Prozesse und Werkstoffe*, Carl Hanser Verlag GmbH Co KG, München **2015**.
[45] F. Lupone, E. Padovano, F. Casamento, C. Badini, *Materials* **2021**, *15*, 183.
[46] K. Wudy, L. Lanzl, D. Drummer, *Phys. Proc.* **2016**, *83*, 991.
[47] M. A. Dechet, J. Schmidt, *Proc. CIRP* **2019**, *94*, 95.
[48] M. A. Dechet, S. Kloos, J. Schmidt, W. Peukert, *AIP Conf. Proc.* **2019**, *2055*, 140002.

[49] D. Rietzel. Werkstoffverhalten und Prozessanalyse beim Laser-Sintern von Thermoplasten. Zugl.: Erlangen-Nürnberg, Univ., Diss., **2011**. Lehrstuhl für Kunststofftechnik, Erlangen, 130 pp.
[50] V. Aravindan, J. Gnanaraj, S. Madhavi, H.-K. Liu, *Chemistry* **2011**, *17*, 14326.
[51] Y. Shi, Z. Li, H. Sun, S. Huang, F. Zeng, *Proc. Instit. Mech. Eng. Part L: J. Mater. Design Appl.* **2004**, *218*, 247.
[52] J. Breuninger, R. Becker, A. Wolf, S. Rommel, A. Verl, *Generative Fertigung mit Kunststoffen: Konzeption und Konstruktion für Selektives Lasersintern*, Springer-Verlag, Berlin, Heidelberg, **2012**.
[53] J. Schmidt, M.A. Dechet, J. S. Gómez Bonilla, N. Hesse, A. Bück, W. Peukert, Characterization of Polymer Powders for Selective Laser Sintering, University of Texas at Austin, **2019**.
[54] G. B. Appetecchi, S. Scaccia, S. Passerini, *J. Electrochem. Soc.* **2000**, *147*, 4448.
[55] Andreas Wegner, **2015**. Theorie über die Fortführung von Aufschmelzvorgängen als Grundvoraussetzung für eine robuste Prozessführung beim Laser-Sintern von Thermoplasten.
[56] M. Launhardt, A. Wörz, A. Loderer, T. Laumer, D. Drummer, T. Hausotte, M. Schmidt, *Polym. Test.* **2016**, *53*, 217.
[57] Wegner Andreas and Gerd Witt, **2012**. Betrachtung zur Pulvernutzungsdauer beim Laser-Sintern und Einfluss der Prozessführung auf die Entstehung von Ausschussbauteilen.
[58] P. B. Bacchewar, S. K. Singhal, P. M. Pandey, *Proc. Instit. Mech. Eng. Part B: J. Eng. Manuf.* **2007**, *221*, 35.
[59] A. Sachdeva, S. Singh, V. S. Sharma, *Int. J. Adv. Manuf. Technol.* **2013**, *64*, 1505.
[60] S. Petzold, J. Klett, A. Schauer, T. A. Osswald, *Polym. Test.* **2019**, *80*, 106094.

How to cite this article: K. Wudy, S. Sapishchuk, J. Hofmann, J. Schmidt, F. Konwitschny, H.-C. Töpper, R. Daub, *J. Appl. Polym. Sci.* **2023**, *140*(14), e53690. https://doi.org/10.1002/app.53690